Structural evidence for pnictogen-centered Lewis acidity in cationic platinum-stibine complexes featuring pendent amino or ammonium groups[†]

Roberta R. Rodrigues [1] and François P. Gabbaï [1,*]   5

[1] Department of Chemistry, Texas A&M University, College Station, Texas 77843-3255, USA; fran-   6
    cois@tamu.edu   7
[*] Correspondence: francois@tamu.edu; Tel.: +1 979 862 2070   8
[†] In memory of Alan H. Cowley, a most inspiring Ph.D. advisor, and a great friend.   9

Abstract: As part of our continuing interest in the chemistry of cationic antimony Lewis acids as   10
ligands for late transition metals, we have now investigated the synthesis of platinum complexes   11
featuring triarylstibine ligand substituted by an *o*-[(dimethylamino)methyl]phenyl group referred   12
to as Ar^N. More specifically, we describe the synthesis of the amino stibine ligand Ph$_2$SbArN (**L**)   13
and its platinum dichloride complex [LPtCl]Cl which exists as a chloride salt and which shows   14
weak coordination of the amino group to the antimony center. We also report the conversion of   15
[LPtCl]Cl into a tricationic complex [LHPt(SMe$_2$)]$^{3+}$ which has been isolated as a tris-triflate salt   16
after reaction of [LPtCl]Cl with SMe$_2$, HOTf and AgOTf. Finally, we show that   17
[LHPt(SMe$_2$)][OTf]$_3$ acts as a catalyst for the cyclization of 2-allyl-2-(2-propynyl)malonate.   18

Keywords: pnictogen bonding, platinum, catalysis   19

1. Introduction

The chemistry of stibines is attracted a renewed interest because of applications in   22
material science and catalysis [1-4]. Although a parallel is often drawn with the ubiq-   23
uitous phosphine ligands, stibines display several atypical traits including redox reac-   24
tions that may occur without dissociation of the coordinated metal [5-10]. Moreover,   25
while phosphines mostly act as two-electron donor spectator ligands, stibines have been   26
shown to display Lewis acidic properties, even when coordinated to a transition metal   27
[11-22]. These Lewis acidic properties manifest in the formation of long contacts be-   28
tween the antimony center of cationic complexes and counteranions as in complex [**A**]$^+$ 29
which was isolated by Reid (Figure 1) [11]. Short contacts, akin to polar covalent bonds,   30
can also be formed in the case of small halide anions, including the fluoride anion [23].   31
Such behavior comes to the fore in the case of complexes featuring bis(phosphino)stibine   32
ligands such as [**B**]$^+$ which is readily converted in **C** in the presence of a fluoride anion   33
(Figure 1) [23].   34

A previous article described the platinum complex D, which features a chloride   36
anion coordinated to the antimony center trans from the platinum atom (Figure 1) [13].   37
The resulting Sb-Cl bond formed by this complex is ~14% longer than the sum of the   38
covalent radii indicating partial ionicity. This lengthening suggested that the simple   39
addition of a donor functionality would suffice in promoting the dissociation of this an-   40
ion, providing access to a cationic complex. Therefore, based on this simple hypothesis,   41
we have decided to replace the antimony-bound phenyl group of **D** by an   42
o-[(dimethylamino)methyl]phenyl group. This substituent is known to form intramo-   43
lecular N-Sb bonds when incorporated in antimony derivatives [24,25] as demonstrated   44

over two decades ago by Cowley, Jones, and Norman [26] as well as by Akiba [27]. In 45
this paper, we report the results of our efforts along with the conversion of the target 46
complex in a triflate derivative that behaves as a carbophilic catalyst. 47
48
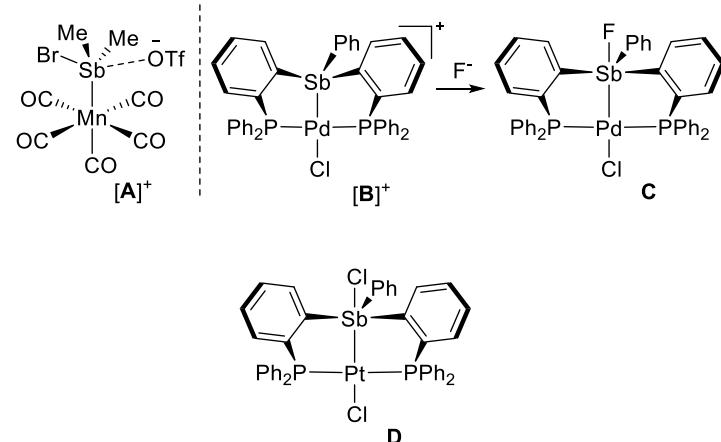
Figure 1. Structure of representative stibine complexes in which the antimony atom displays Lewis 50
acidic properties. 51

2. Results and discussion 52

As a first step, we decided to introduce the *o*-[(dimethylamino)methyl]phenyl group 53
by reaction of the corresponding lithium salt [27] with the bis(phosphino)chlorostibine **1** 54
[28] as shown in Scheme 1. The reaction was carried out in toluene upon heating to 55
80°C. Following standard workup and column chromatography, the new ami- 56
no-functionalized ligand **2** was obtained as an air-stable solid in 71%. The presence of 57
o-[(dimethylamino)methyl]phenyl group could be easily confirmed by ^{1}H NMR spec- 58
troscopy, which displayed resonances at 1.69 ppm and 3.37 ppm (in C_6D_6) corresponding 59
to the benzylic methylene and dimethylamino groups, respectively. Integration of these 60
two resonances produced the expected intensity ratio when referenced to the resonances 61
arising from the phenylene protons in the aromatic region of the spectrum. The pres- 62
ence of the phopshino groups was easily confirmed by the detection of a single resonance 63
at -8.19 ppm in the ^{31}P NMR spectrum. 64
65
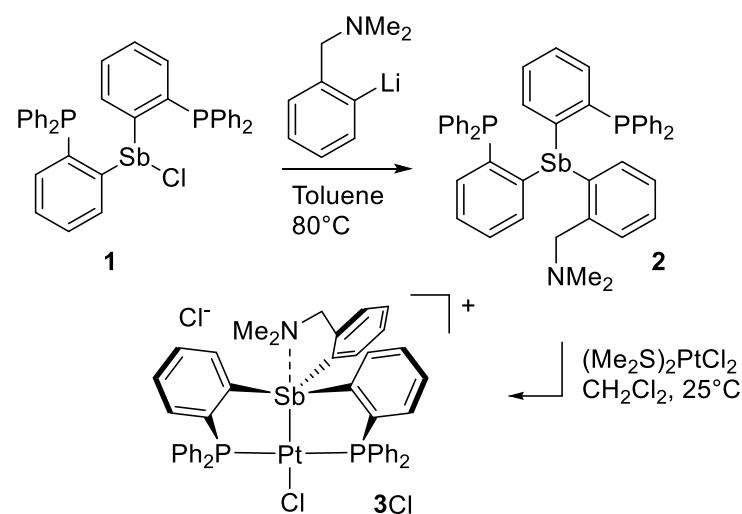
Scheme 1. Synthesis of ligand **2** and its conversion into the corresponding platinum(II) complex 67
[**3**][Cl]. 68

With this ligand at our disposal, we decided to investigate its reaction (Me$_2$S)$_2$PtCl$_2$. This reaction, which was carried out in CH$_2$Cl$_2$ at room temperature, proceeded smoothly to afford complex [3][Cl] as an air-stable solid in 89% yield. The ^{31}P NMR spectrum of complex [3][Cl] features a resonance at 49.52 ppm that features the expected ^{195}Pt satellites. The $^{1}J_{Pt-P}$ coupling constant of 2,524 Hz is comparable to that measured for complex **D** ($^{1}J_{Pt-P}$ = 2,706 Hz), suggesting the formation of a divalent square planar platinum complex. Other notable spectroscopic features include a downfield of the phenylene proton positioned ortho from the antimony atom from 7.50 ppm in **2** to 8.37 ppm in [3][Cl]. Finally, the benzylic methylene and dimethylamino group give rise to sharp resonances at 1.71 ppm and 3.10 ppm, respectively. Because the chemical shift of these resonances is close to those in the free ligand **2**, we resorted to X-ray analysis to elucidate the antimony atom's coordination environment in [3][Cl] and the eventual presence of dative N→Sb dative interaction.
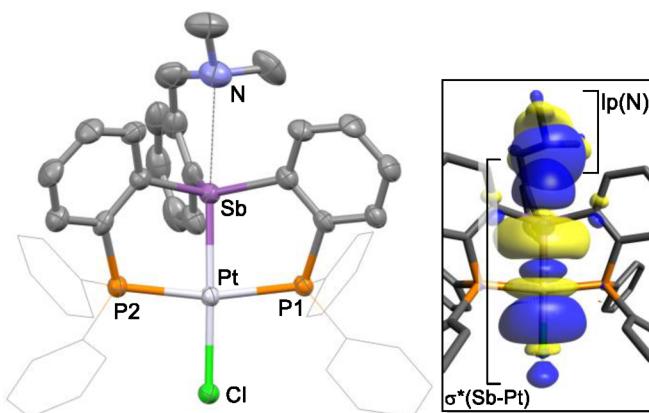
Figure 2: Solid-state structure of complex [3][Cl]. Thermal ellipsoids are drawn at the 50 % probability level. The hydrogen atoms, interstitial solvent molecules, and counteranions are omitted for clarity while the Ph groups are draw as thin lines.. Relevant metrical parameters can be found in the text.

Single crystals of complex [3][Cl] could be easily obtained upon diffusion of pentane into a CH$_2$Cl$_2$ of [3][Cl] at ambient temperature in air. Complex [3][Cl] crystallizes in the *P*2$_1$/*c* space group with one molecule in the asymmetric unit (Table 1, Figure 2). Inspection of the solid-state structure indicates the formation of a cationic complex formed by complete ionization of the Sb-Cl bond, resulting in the presence of a chloride counter anion sitting in the lattice and forming a hydrogen bond with an adventitious water molecule. The cationic complex [3]$^+$ possesses platinum in a square planar geometry with a chloride ligand coordinated trans from the antimony atom as in the case of **D** [13]. The resulting Sb-Pt bonds of 2.4928(5) A° is notably shorter than that in **D** (2.5380(8) Å). This shortening can be correlated to the absence of an antimony-bound chloride ligand in the case of [3][Cl]. Indeed, at first glance, the antimony moiety of [3]$^+$ corresponds to a rather classical platinum-coordinated stibine unit. In support of this formulation, we note that the Sb-Pt bond in [3][Cl] is comparable to that found in classical coordination complexes such as *cis*-[PtCl$_2$(SbPh$_3$)$_2$] (av. 2.50 Å) [29]. The Pt-Cl distance of 2.3621(15) Å is slightly shorter than that in **D** (2.3851(16) A), indicating that the platinum center of [3][Cl] is slightly more electrophilic than in **D**. Finally, we note that the nitrogen of the amino group sits at 2.962(7) Å from the antimony center.

Table 1. Crystal data and structure refinement for [3][Cl] and [4]OTf$_3$.^{1}

	[3][Cl]-(CH$_2$Cl$_2$)$_2$-(H$_2$O)	[4]OTf$_3$-MeCN
Empirical formula	C$_{47}$H$_{46}$Cl$_6$NOP$_2$PtSb	C$_{52}$H$_{50}$F$_9$N$_2$O$_9$P$_2$PtS$_4$Sb
M	1232.33 g/mol	1524.96 g/mol

Temperature	110 K	110.0 K
Wavelength	1.54178 Å	0.71073 Å
Crystal system	Monoclinic	Monoclinic
Space group	$P2_1/c$	$P2_1/c$
Unit cell dimensions	$a = 11.0507(5)$ Å	$a = 13.2984(15)$ Å
	$b = 18.1574(8)$ Å	$b = 14.3100(17)$ Å
	$c = 24.0847(11)$ Å	$c = 30.743(3)$ Å
	$\beta = 99.231(2)°$	$\beta = 101.601(3)°$
Volume	4770.1(4) Å^3	5730.9(11) Å^3
Z	4	4
Density (calculated)	1.716 g/cm^3	1.767 g/cm^3
Absorption coefficient	13.906 mm^{-1}	3.196 mm^{-1}
Θ range	3.062 to 66.593°.	1.963 to 28.281°.
Reflections collected	56128	126808
Independent reflections	8379 [$R_{int} = 0.0648$]	14206 [$R_{int} = 0.0639$]
Goodness-of-fit on F^2	1.065	1.081
R indices (all data)	$R_1 = 0.0494$, $wR_2 = 0.1206$	$R_1 = 0.0530$, $wR_2 = 0.0853$

[1] Additional details are available in the CIF files that have been deposited with the CCCDC.

This distance is longer than that measured in **E** [30] or **F** [26], which possess N→Sb dative interactions of 2.693(11) Å and 2.463(2) Å, respectively (Figure 3). Based on this comparison, we conclude that an N→Sb dative interaction is also present in [**3**][Cl], even if weaker than in **E** and **F**. Efforts to reproduce the experimental geometry with DFT methods have not been successful and have led to computed structures where the Sb-N distance is overestimated by ~0.3 Å. We assign our difficulty in reproducing this distance to its inherent weakness. An optimization carried out with the MPW1PW91 functional, a mixed basis set, and application of a solvation model afforded a N-Sb distance of 3.26 Å. Despite this elongation, an NBO analysis of the bonding indicates the persistence of an N→Sb dative interaction that accounts for $E_{del} = 8.0$ kcal/mol to the stability of the molecule (Figure 2).
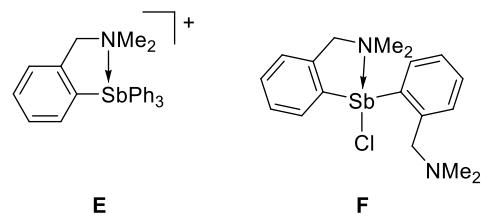

Figure 3: Selected examples of derivatives with N→Sb dative interactions.

Given these results, we became eager to verify if this interaction is nonetheless sufficient to promote dissociation of the chloride anion from the antimony atom in solution. To this end, we decided to carry out conductance measurements in CH$_2$Cl$_2$ solution. In keeping with literature precedents, we decided to carry out these measurements with solution containing 1 mM concentration of the species [31]. We first benchmarked our technique using Ph$_3$SbCl$_2$ and [Ph$_4$Sb][OTf] [32], which afforded molar conductivities (Λ_M) of 0.26 and 48.4 S·cm^2 mol^{-1}, respectively. These results indicate that Ph$_3$SbCl$_2$ does not dissociate under these conditions while [Ph$_4$Sb][OTf] behaves as a 1:1 electrolyte. Next, we compared complex **D** and [**3**][Cl] and observed a contrasting behavior. Indeed while **D** showed a low conductivity 18.52 S cm^2 mol^{-1}, [**3**][Cl] displayed a molar conductance of 52.4 S·cm^2 mol^{-1}, close to that of [Ph$_4$Sb][OTf] indicating that [**3**][Cl] is also 1:1 electrolyte. To ascertain this conclusion, we also measured the conductance of [Ph$_4$Sb][OTf] and [**3**][Cl] at 0.5 and 0.1 mmol. Via extrapolation of the resulting data

points to infinite concentrations, we obtained $\Lambda°$ values of 138 S cm^2 mol^{-1} for [Ph$_4$Sb][OTf] and 120 S cm^2 mol^{-1} for [**3**][Cl]. These values match the range determined for similar 1:1 electrolytes in organic solvents [33]. These experiments indicate that, despite the weakness of the N-Sb interaction, the presence of a dimethylamino-methylene group is sufficient to drive the heterolytic dissociation of the Sb-Cl bond both in solution as well as in the solid-state.

In prior studies, we have observed that antimony platinum triflate complexes are endowed with attractive carbophilic reactivity [34,35]. Encouraged by these recent findings, we attempted to convert [**3**][Cl] into the corresponding bis(triflate) derivative. This reaction proved inconsistent and failed to deliver the targeted bis(triflate). In one of these reactions, which was carried out by treating a crude batch of **2** with AgOTf, a small crop of crystals of a new complex was isolated. X-ray analysis of these crystals revealed the formation of a tricationic complex isolated as a triflate salt (Table 1, Figure 4). The structure of this new salt, referred to as [**4**][OTf]$_3$, also showed protonation of the nitrogen atom as well as the presence a dimethylsulfide ligand bound to the platinum center. Because of its protonation, the nitrogen atom is no longer involved in a donor-acceptor interaction with the antimony atom. The latter adopts a distorted tetrahedral geometry and is coordinated to the square planar platinum atom, trans from the site occupied by the Me$_2$S ligand. The resulting Sb-Pt distance of 2.4929(3) Å is almost identical to that in [**3**][Cl]. The dimethylsulfide ligand is bound to the platinum atom via a Pt-S distance of 2.3864(2) Å which can be compared to the value of 2.3611(8) Å measured in the cationic complex [κ^2-2-*N*Me$_2$-3-*P^i*Pr$_2$-indene)PtMe(SMe$_2$)]$^+$ [36]. Finally, the ammonium group forms a hydrogen bonding interaction with one of the triflate counter anions (Figure 4). This triflate counter anion is also involved in a long Sb-O contact of 3.215(3) Å, along the direction of the Sb-Pt bond. Another triflate anion approaches the antimony center along the direction defined by the Sb-C$_{Ph}$ bond, leading to another Sb-O contact of 3.229(4) Å. These contacts are reminiscent of those observed in the structure of complexes such as **A**.

O-N: 2.861(5) Å
Sb-O1: 3.215(3) Å
Sb-O2: 3.229(4) Å
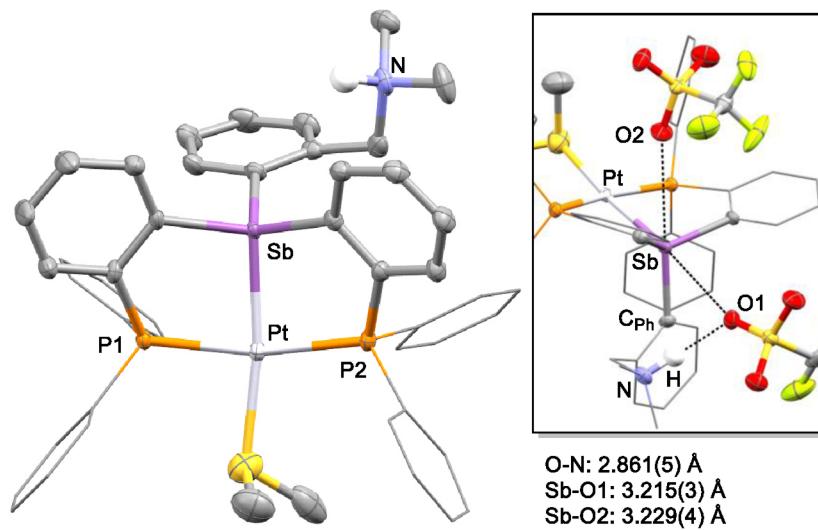
Figure 4: Solid-state structure of complex [**4**][OTf]$_3$. Thermal ellipsoids are drawn at the 50 % probability level. The hydrogen atoms, interstitial solvent molecules, and counteranions are omitted for clarity while the Ph groups are draw as thin lines. The inset shows weak interactions involving the triflate anions along with selected distances. Other relevant metrical parameters can be found in the text.

The presence of a Me$_2$S ligand in [**4**][OTf]$_3$ suggested it was present as an impurity in the crude batch **2** used in the experiment. Aiming for a reproducible and higher-yielding

synthesis of [**4**][OTf]$_3$, [**3**][Cl] was treated with AgOTf (6 equiv.) in the presence of triflic acid and dimethyl sulfide (Scheme 2). This procedure afforded [**4**][OTf]$_3$ in a 45% yield. The ^{31}P NMR spectrum of [**4**][OTf]$_3$ features a single resonance at 50.65 ppm coupled to the ^{195}Pt nuclei by $^1J_{Pt–P}$ = 3,020 Hz. This value, although larger than that for [**3**][Cl] remains consistent with the existence of a divalent platinum center. In the ^{1}H NMR spectrum, the phenylene proton positioned ortho from the antimony atom appears at 8.75 ppm, a value that can be compared to that of 8.37 ppm measured for [**3**][Cl]. The benzylic methylene group is observed at 2.78 ppm, while the nitrogen-bound methyl group gives rise to a doublet ($^3J_{H-H}$ = 5.0 Hz) at 2.07 ppm. The ammonium proton gives rise to a broad signal at 6.94 ppm. Freshly prepared crystals of [**4**][OTf]$_3$ show a resonance at 1.76 ppm assigned to the dimethylsulfide ligand. The coordination of this ligand to the platinum center is confirmed by the detection of ^{195}Pt satellites spaces by a $^3J_{Pt-H}$ coupling constant of 43.9 Hz. This value is comparable to that of 36.5 Hz reported for [κ^2-2-NMe$_2$-3-P^iPr$_2$-indene)PtMe(SMe$_2$)]$^+$ [36].
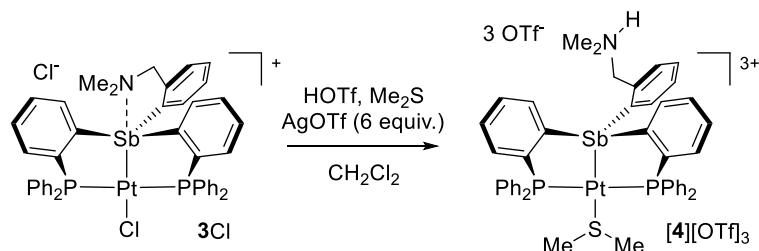
Scheme 2: Synthesis of [**4**][OTf]$_3$.

To conclude this study, we tested the catalytic activity of [**4**][OTf]$_3$ in the cycloisomerization of 2-allyl-2-(2-propynyl)malonate, a reaction type well known to be promoted by electrophilic platinum catalysts [19,34,37,38]. We found that the reaction proceeded in CD$_2$Cl$_2$ when carried out in a sealed NMR tube at 50°C (Scheme 3). With a catalyst loading of 5 mol%, monitoring of the reaction by ^{1}H NMR spectroscopy showed the formation of the five-membered isomer with a conversion greater than 90% after 3 hours. When the same reaction was attempted with [**3**][Cl], no conversion was observed even after 24 h, at the same temperature. This difference underscores the advantages gained by introduction of triflate counterions. Finally, we will note the parallel that exists between [**4**][OTf]$_3$ and [(o-(Ph$_2$P)C$_6$H$_4$)$_2$SbOTf$_2$]PtCl (**G**), which also promotes such enyne cyclization reactions, albeit at room temperature [34]. The higher temperature needed in the case of [**4**][OTf]$_3$ is tentatively assigned to the presence of a Me$_2$S ligand which tames the reactivity of the platinum center.
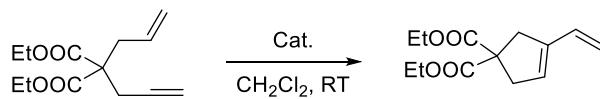
Scheme 3: Enyne cyclization reaction used to benchmark the catalytic activity of the complexes.

3. Materials and Methods

3.1. General experimental considerations

Compound **1** and PtCl$_2$(SMe$_2$)$_2$ was prepared according to the reported procedure [28,39]. Toluene and Et$_2$O were dried by reflux under N over Na/K and distilled before use. MeCN and CH$_2$Cl$_2$ were dried over CaH$_2$ and distilled before use. Pentane was dried over activated molecular sieves. All other solvents were used as received. Commercially

available chemicals were purchased and used as provided (Commercial sources: Aldrich for $SbCl_3$; Matrix Scientific for AgOTf). Ambient temperature NMR spectra were recorded on a Bruker Avance 400 or 500 FT NMR (499.42 MHz for ^1H, 125.62 MHz for ^{13}C, 469.89 MHz for ^{19}F, 202.16 MHz for ^{31}P). ^1H and ^{13}C NMR chemical shifts are given in ppm and are referenced against $SiMe_4$ using residual solvent signals used as secondary standards. Elemental analyses (EA) were performed at Atlantic Microlab (Norcross, GA).

3.2. Synthesis of compound 2

Compound **1** (344 mg, 0.51 mmol) and (2-((dimethylamino)methyl)phenyl)lithium were dissolved in toluene (2 mL). The resulting mixture was heated to 80 °C for 12 hours. The solution was filtered, and the solvent evaporated. The crude product was purified by column chromatography using 10-20% ethyl acetate/hexanes to afford **2** as a white solid (280 mg, 71% yield). ^1H NMR (400 MHz; C_6D_6): δ 7.60-7.34 (m, 3H), 7.35-7.25(m, 9H), 7.02 – 6.95 (m, 19H), 6.90 (t, 1H, $^3J_{H-H}$ = 8.0 Hz), 3.37 (s, 2H), 1.69 (s, 6.00 H). $^{13}C\{^1H\}$ NMR (125.62 MHz; C_6D_6): δ 153.2 (dd, J_{C-P} = 55.7 Hz), 144.22 (s), 144.17 (d, J_{C-P} = 4.8 Hz), 142.80 (t, J_{C-P} = 12.9 Hz),138.12 (s), 137.66 (d, J_{C-P} = 14.1 Hz), 137.05 (d, J_{C-P} = 14.1 Hz), 136.42 (d, J_{C-P} = 14.1 Hz), 133.30 (d, J_{C-P} = 20.7 Hz), 133.12 (s), 132.67 (d, J_{C-P} = 20.7 Hz), 128.23 (s), 64.92 (s), 43.17 (s). $^{31}P\{^1H\}$ NMR (161.74 MHz; C_6D_6): δ -8.19. This compound was not subjected to combustion analysis. The reported yield is thus a crude yield.

3.3. Synthesis of [3][Cl]

Compound **2** (527 mg, 0.68 mmol) and $PtCl_2(SMe_2)_2$ (245 mg, 0.63 mmol) were combined in CH_2Cl_2 (2 mL). After stirring at room temperature for 12 hours, the solvent was removed under vacuum and the crude residue was dissolved in CH_2Cl_2 (1 mL). The resulting solution was added dropwise to 10 mL of Et_2O which resulted in the precipitation of [**3**][Cl] as a light yellow solid. This compound was isolated by filtration and dried under vacuum. This procedure afforded [**3**][Cl] in a crude yield of 96% yield (630 mg). ^1H NMR (400 MHz; $CDCl_3$): δ 8.37 (d, 2H, o-P(Sb)C_6H_4, $^3J_{H-H}$ = 8.0 Hz), 7.90 (t, 2H, $^3J_{H-H}$ = 8.0 Hz), 7.67 - 7.52 (m, 6H), 7.50 - 7.28 (m, 16H), 7.27-7.24 (m, 3H), 7.01 (d, 1H, $^3J_{H-H}$ = 8.0 Hz), 6.90 (d, 1H, $^3J_{H-H}$ = 8 Hz), 6.82 (t, 1H, $^3J_{H-H}$ = 8.0 Hz), 3.10 (s, 2H), 1.71 (s, 6H). $^{13}C\{^1H\}$ NMR (125.62 MHz; $CDCl_3$): δ 141.06 (s), 140.51 (t, J_{C-P} = 19.7 Hz), 138.94 (t, J_{C-P} = 30.3 Hz), 136.77 (s), 136.12 (brs), 135.76 (t, J_{C-P} = 9.2 Hz), 134.06 (m), 132.72 (brs), 132.28 (s), 132.18 (s), 131.88 (s), 129.46 (t, J_{C-P} = 5.6 Hz), 128.94-128.60 (m), 128.34 (s), 128.13 (brs), 127.91 (s), 127.66 (s), 126.52 (s), 63.02 (s), 45.87 (s). $^{31}P\{^1H\}$ NMR (161.74 MHz; $CDCl_3$): δ 49.52 (s, $^1J_{Pt-P}$ = 2706 Hz). The compound could be recrystallized by diffusion of pentane into a CH_2Cl_2 of [**3**][Cl] at ambient temperature in air. This procedure afforded crystals of [**3**][Cl] with two interstitial molecules of CH_2Cl_2 and one molecule of water as established by X-ray diffraction. A portion of the recrystalized sample was subjected to combustion analysis, which afforded the following results. Elemental analysis calcd (%) for $C_{45}H_{40}Cl_2NP_2PtSb-H_2O-0.5(CH_2Cl_2)$: C: 49.46, H: 3.92; found: C 49.50, H: 3.95. These combustion analysis results suggest the presence of interstitial water and CH_2Cl_2, with the latter being partly depleted, presumably as a result of solvent loss during shipping.

3.4. Synthesis of [4][OTf]₃

Salt [**3**][Cl] (100 mg, 0.10 mmol) was dissolved in CH_2Cl_2 (1ml) and treated with AgOTf (148 mg, 0.58 mmol) under an N_2 atmosphere. The reaction mixture was allowed to stir for 2 hours then one drop of trifluoromethanesulfonic acid and one drop of dimethyl sulfite was added to the reaction mixture. The reaction mixture was then allowed to stir for 12 hours. The AgCl precipitate was filtered with 0.45 um PTFE syringe filter and the product was isolated by vapor diffusion of Et_2O (2 mL) into MeCN to yield colorless crystals (70 mg, 48% yield) suitable for X-ray diffraction. ^1H NMR (400 MHz; CD_3CN): δ 8.92 (d, 2H, o-P(Sb)C_6H_4, $^3J_{H-H}$ = 8.0 Hz), 8.20 (brs, 1H) 7.96 (t, 2H, $^3J_{H-H}$ = 8.0 Hz), 7.92 - 7.81 (m, 4H), 7.80 -7.56 (m, 21H), 7.45-7.37(m, 2H), 6.70 (t, 1H, $^3J_{H-H}$ = 4.0 Hz), 6.12 (d, 1H, $^3J_{H-H}$ =

8.1 Hz), 2.76 (d, 6H, $^3J_{H-H}$ = 5.0 Hz), 2.20 (d, 6H, $^3J_{H-H}$ = 5.0 Hz), 1.76 (s, 6H, $^3J_{Pt-H}$ = 43.9 Hz). ^{13}C{^{1}H} NMR (125.62 MHz; CDCl$_3$): δ 142.02 (t, J_{C-P} = 34.0 Hz), 137.89 (t, J_{C-P} = 7.6 Hz), 136.46 (brs), 135.79 (t, J_{C-P} = 7.7 Hz), 135.46 (s), 135.31-134.98 (m), 134.64 (brs), 134.56 (s), 134.36 (t, J_{C-P} = 6.64 Hz), 134.06 (s), 132.90 (s), 132.85 (s), 131.61 (s), 131.56 (s), 131.53 (s), 130.47 (t, J_{C-P} = 5.6 Hz), 126.12 (t, J_{C-P} = 29.8 Hz), 125.50 (t, J_{C-P} = 29.6 Hz), 122.15 (s), 119.60 (s), 117.05 (s), 116.94 (s), 60.13 (s), 42.84 (s), 23.21 (s). ^{31}P{^{1}H} NMR (161.74 MHz; CDCl$_3$): δ 50.65 (s, $^1J_{Pt-P}$ = 3020 Hz). Elemental analysis calcd (%) for C$_{48}$H$_{41}$F$_9$NO$_9$P$_2$PtS$_3$Sb: C: 40.47, H: 3.9; found: C 40.38, H: 3.32.

3.5. Conductance measurements

Conductance measurements were carried out in CH$_2$Cl$_2$ at concentrations using a Mettler Toledo FiveGo conductivity probe. All compounds were first measured at 1 mM concentrations. In the case of [Ph$_4$Sb][OTf] and [**3**][Cl], conductance measurements were carried out at three concentrations affording: at 1 mM, 0.5 mM, and 0.1 mM, affording the following conductance values: 48.4 μS cm^{-1} at 1 mM, 28.8 μS cm^{-1} at 0.5 mM, and 9.22 μS cm^{-1} at 0.1 mM for Ph$_4$SbOTf; 52.4 μS cm^{-1} at 1 mM, 29.0 μS cm^{-1} at 0.5 mM, and 8.4 μS cm^{-1} at 0.1 mM for [**3**][Cl]. The Λ° molar conductivity values were obtained by plotting the conductance data as a function of the square root of the concentration and by extrapolating to infinite dilution.

3.6. Crystallographic measurements

The crystallographic measurements were performed at 110(2) K using a Bruker Venture diffractometer ([**3**][Cl]) (Cu K$_α$ radiation, $λ$ = 1.54178 Å) and a Bruker Quest diffractometer for [**4**][OTf]$_3$ (Mo K$_α$ radiation, $λ$ = 0.71073 Å). In each case, a specimen of suitable size and quality was selected and mounted onto a nylon loop and cooled to 110(2) K in a cold nitrogen stream (OXFORD Crysosystems). The data were collected and reduced using Bruker AXS APEX 3 software [40] and solved by direct methods. Semiempirical absorption corrections were applied using SADABS [41]. Subsequent refinement were carried with the the SHELXTL/PC package (version 6.1 & OLEX^2) [42,43]. Thermal parameters were refined anisotropically for all non-hydrogen atoms to convergence. Hydrogen atoms were added at idealized positions using a riding model. CCDC 2067400 ([**3**][Cl]) and 2067401 ([**4**][OTf]$_3$) contains the supplementary crystallographic data for this paper. These data can be obtained free of charge via http://www.ccdc.cam.ac.uk/conts/retrieving.html (or from the CCDC, 12 Union Road, Cambridge CB2 1EZ, UK; Fax: +44 1223 336033; E-mail: deposit@ccdc.cam.ac.uk.

3.7. DFT calculations

The structure of complex [**3**]$^+$ was optimized using DFT methods in Gaussian 09 [44]. In all cases, the crystal structure of derivative was chosen as a starting point and the Polarizable Continuum Model (PCM) (solvent = water) was applied during the optimization. The following level of theory was employed: MPW1PW91 functional and a mixed basis set (cc-pVTZ-PP for Pt and Sb; 6-311G(d,p) for H/C/N/P/Cl). Frequency calculations, performed at the same level of theory with application of the PCM (solvent = acetonitrile), found no imaginary frequencies. NBO analysis was performed with the NBO 6.0 program [45] using the same level of theory as in the optimization.

4. Conclusions

The results presented in this study show that the inclusion of a pendent dimethylamino group positioned next to the antimony center of [**3**][Cl] promotes chloride anion dissociation from the antimony center, facilitating cation formation. As indicated by the isolation of [**4**][OTf]$_3$, this amino group can also be readily protonated without compromising the PtSb dinuclear core's integrity. Although the carbophilic reactivity of [**4**][OTf]$_3$ suffers from the presence of a Me$_2$S ligand bound to the platinum center, the

inclusion of a donor amino functionality may present advantages. Indeed, we speculate that such a functionality could relay protons during catalysis and possibly facilitate protodematellation steps, a possibility we are investigating by attempting the incorporation of ligand **2** in complexes with exposed late transition metals. Finally, the electron-deficient characteristics of [**4**][OTf]$_3$ manifest in the formation of two long Sb-O$_{triflate}$ contacts speaking to the Lewis acidic or pnictogen-bond donor properties of the antimony atom in this structure.

Supplementary Materials: Figure S1: ^{1}H NMR of compound **2** in C$_6$D$_6$, Figure S2: ^{13}CNMR of compound **2** in C$_6$D$_6$, Figure S3: ^{31}PNMR spectrum of compound **2** in C$_6$D$_6$, Figure S4:^{1}HNMR spectrum of compound [**3**][Cl] in CDCl$_3$, Figure S5: ^{31}PNMR spectrum of compound [**3**][Cl] in CDCl$_3$, Figure S6:^{13}CNMR spectrum of compound [**3**][Cl] in CDCl$_3$, Figure S7:^{1}HNMR spectrum of compound [**4**][OTf]$_3$ in CD$_2$Cl$_2$, Figure S8: ^{13}CNMR spectrum of compound [**4**][OTf]$_3$ in CD$_2$Cl$_2$, Figure S9: ^{31}PNMR spectrum of [**4**][OTf]$_3$ in CD$_2$Cl$_2$, Figure S10: ^{1}HNMR spectra of collected during the cyclization of 2-allyl-2-(2-propynyl)malonate catalyzed by [**4**][OTf]$_3$ (5 mol%) in CD$_2$Cl$_2$ at 50°C, Figure S11: Selected Natural Bond Orbitals involved in the N→Sb interaction present in the [**3**]$^+$, Table S1. Cartesian coordinates (in Å) for the optimized structure of [**3**]$^+$.

Author Contributions: RRR carried out the experimental work and co-designed the study with FPG.

Conflicts of Interest: The authors declare no conflict of interest.

Sample Availability: The compounds described in this paper were not synthesized in sufficiently large quantities to be available for distribution.

References

1. Schulz, S. The chemistry of Group 13/15 compounds (III-V compounds) with the higher homologues of Group 15, Sb and Bi. *Coord. Chem. Rev.* **2001**, *215*, 1.

2. Levason, W.; Reid, G. Developments in the coordination chemistry of stibine ligands. *Coord. Chem. Rev.* **2006**, *250*, 2565.

3. Burt, J.; Levason, W.; Reid, G. Coordination chemistry of the main group elements with phosphine, arsine and stibine ligands. *Coord. Chem. Rev.* **2014**, *260*, 65.

4. Greenacre, V. K.; Levason, W.; Reid, G. Developments in the chemistry of stibine and bismuthine complexes. *Coord. Chem. Rev.* **2021**, *432*, 213698.

5. Wade, C. R.; Gabbaï, F. P. Two-Electron Redox Chemistry and Reversible Umpolung of a Gold–Antimony Bond. *Angew. Chem. Int. Ed.* **2011**, *50*, 7369.

6. Jones, J. S.; Wade, C. R.; Gabbaï, F. P. Redox and anion exchange chemistry of a stibine nickel complex: Writing the L, X, Z ligand alphabet with a single element. *Angew. Chem. Int. Ed.* **2014**, *53*, 8876.

7. Jones, J. S.; Wade, C. R.; Gabbaï, F. P. Guilty on Two Counts: Stepwise Coordination of Two Fluoride Anions to the Antimony Atom of a Noninnocent Stibine Ligand. *Organometallics* **2015**, *34*, 2647.

8. Jones, J. S.; Gabbaï, F. P. Coordination- and Redox-Noninnocent Behavior of Ambiphilic Ligands Containing Antimony. *Acc. Chem. Res.* **2016**, *49*, 857.

9. Sen, S.; Ke, I.-S.; Gabbaï, F. P. T-Shaped Gold→Stiborane Complexes as Carbophilic Catalysts: Influence of the Peripheral Substituents. *Organometallics* **2017**, *36*, 4224.

10. Wächtler, E.; Oro, L. A.; Iglesias, M.; Gerke, B.; Pöttgen, R.; Gericke, R.; Wagler, J. Synthesis and Oxidation of a Paddlewheel-Shaped Rhodium/Antimony Complex Featuring Pyridine-2-Thiolate Ligands. *Chem. Eur. J.* **2017**, *23*, 3447.

11. Benjamin, S. L.; Levason, W.; Reid, G.; Warr, R. P. Halostibines $SbMeX_2$ and $SbMe_2X$: Lewis Acids or Lewis Bases? *Organometallics* **2012**, *31*, 1025.

12. Benjamin, S. L.; Levason, W.; Light, M. E.; Reid, G.; Rogers, S. M. Bromostibine Complexes of Iron(II): Hypervalency and Reactivity. *Organometallics* **2014**, *33*, 2693.

13. Ke, I.-S.; Jones, J. S.; Gabbaï, F. P. Anion-Controlled Switching of an X Ligand into a Z Ligand: Coordination Non-innocence of a Stiboranyl Ligand. *Angew. Chem. Int. Ed.* **2014**, *53*, 2633.

14. Sen, S.; Ke, I.-S.; Gabbaï, F. P. Anion-Controlled Positional Switching of a Phenyl Group about the Dinuclear Core of a AuSb Complex. *Inorg. Chem.* **2016**, *55*, 9162.

15. Jones, J. S.; Wade, C. R.; Yang, M.; Gabbaï, F. P. On the coordination non-innocence of antimony in nickel(II) complexes of the tetradentate (*o*-(Ph$_2$P)C$_6$H$_4$)$_3$Sb ligand. *Dalton Trans.* **2017**, *46*, 5598.

16. Jones, J. S.; Gabbaï, F. P. Activation of an Au-Cl Bond by a Pendent Sb^{III} Lewis Acid: Impact on Structure and Catalytic Activity. *Chem. Eur. J.* **2017**, *23*, 1136.

17. Plajer, A. J.; Colebatch, A. L.; Rizzuto, F. J.; Pröhm, P.; Bond, A. D.; García-Rodríguez, R.; Wright, D. S. How Changing the Bridgehead Can Affect the Properties of Tripodal Ligands. *Angew. Chem. Int. Ed.* **2018**, *57*, 6648.

18. Jolleys, A.; Lake, B. R. M.; Krämer, T.; Benjamin, S. L. A Five-Membered PdSb$_n$ Coordination Series. *Organometallics* **2018**, *37*, 3854.

19. You, D.; Yang, H.; Sen, S.; Gabbaï, F. P. Modulating the σ-Accepting Properties of an Antimony Z-type Ligand via Anion Abstraction: Remote-Controlled Reactivity of the Coordinated Platinum Atom. *J. Am. Chem. Soc.* **2018**, *140*, 9644.

20. Furan, S.; Hupf, E.; Boidol, J.; Brünig, J.; Lork, E.; Mebs, S.; Beckmann, J. Transition metal complexes of antimony centered ligands based upon acenaphthyl scaffolds. Coordination non-innocent or not? *Dalton Trans.* **2019**, *48*, 4504.

21. Gericke, R.; Wagler, J. Ruthenium Complexes of Stibino Derivatives of Carboxylic Amides: Synthesis and Characterization of Bidentate Sb,E, Tridentate Sb,E$_2$, and Tetradentate Sb,E$_3$ (E = N and O) Ligands and Their Reactivity Toward [RuCl$_2$(PPh$_3$)$_3$]. *Inorg. Chem.* **2020**, *59*, 6359.

22. Wachtler, E.; Gericke, R.; Block, T.; Pottgen, R.; Wagler, J. Trivalent Antimony as L-, X-, and Z-Type Ligand: The Full Set of Possible Coordination Modes in Pt-Sb Bonds. *Inorg. Chem.* **2020**, *59*, 15541.

23. Wade, C. R.; Ke, I.-S.; Gabbaï, F. P. Sensing of Aqueous Fluoride Anions by Cationic Stibine–Palladium Complexes. *Angew. Chem. Int. Ed.* **2012**, *51*, 478.

24. Opris, L. M.; Silvestru, A.; Silvestru, C.; Breunig, H. J.; Lork, E. Solid-state structure and solution behaviour of hypervalent organoantimony halides containing 2-(Me$_2$NCH$_2$)C$_6$H$_4$– moieties. *Dalton Trans.* **2003**, *32*, 4367.

25. Sharma, P.; Castillo, D.; Rosas, N.; Cabrera, A.; Gomez, E.; Toscano, A.; Lara, F.; Hernández, S.; Espinosa, G. Synthesis and structures of organoantimony compounds containing intramolecular Sb–N interactions. *J. Organomet. Chem.* **2004**, *689*, 2593.

26. Carmalt, C. J.; Cowley, A. H.; Culp, R. D.; Jones, R. A.; Kamepalli, S.; Norman, N. C. Synthesis and Structures of Intramolecularly Base-Coordinated Group 15 Aryl Halides. *Inorg. Chem.* **1997**, *36*, 2770.

27. Yamamoto, Y.; Chen, X.; Kojima, S.; Ohdoi, K.; Kitano, M.; Doi, Y.; Akiba, K.-Y. Experimental Investigation on Edge Inversion at Trivalent Bismuth and Antimony: Great Acceleration by Intra- and Intermolecular Nucleophilic Coordination. *J. Am. Chem. Soc.* **1995**, *117*, 3922.

28. Yang, H.; Gabbaï, F. P. Solution and Solid-State Photoreductive Elimination of Chlorine by Irradiation of a [PtSb]^{VII} Complex. *J. Am. Chem. Soc.* **2014**, *136*, 10866.

29. Wendt, O. F.; Scodinu, A.; Elding, L. I. Trans influence of triphenylstibine. Crystal and molecular structures of cis-[PtCl2(SbPh3)2] and trans-[PtI2(SbPh3)2]. *Inorg. Chim. Acta* **1998**, *277*, 237.

30. Yang, M.; Pati, N.; Belanger-Chabot, G.; Hirai, M.; Gabbaï, F. P. Influence of the catalyst structure in the cycloaddition of isocyanates to oxiranes promoted by tetraarylstibonium cations. *Dalton Trans.* **2018**, *47*, 11843.

31. Geary, W. J. The use of conductivity measurements in organic solvents for the characterisation of coordination compounds. *Coord. Chem. Rev.* **1971**, *7*, 81.

32. Robertson, A. P. M.; Chitnis, S. S.; Jenkins, H. A.; McDonald, R.; Ferguson, M. J.; Burford, N. Establishing the Coordination Chemistry of Antimony(V) Cations: Systematic Assessment of Ph$_4$Sb(OTf) and Ph$_3$Sb(OTf)$_2$ as Lewis Acceptors. *Chem. Eur. J.* **2015**, *21*, 7902.

33. LeSuer, R. J.; Buttolph, C.; Geiger, W. E. Comparison of the Conductivity Properties of the Tetrabutylammonium Salt of Tetrakis(pentafluorophenyl)borate Anion with Those of Traditional Supporting Electrolyte Anions in Nonaqueous Solvents. *Anal. Chem.* **2004**, *76*, 6395.

34. You, D.; Gabbaï, F. P. Unmasking the Catalytic Activity of a Platinum Complex with a Lewis Acidic, Non-innocent Antimony Ligand. *J. Am. Chem. Soc.* **2017**, *139*, 6843.

35. You, D.; Smith, J. E.; Sen, S.; Gabbaï, F. P. A Stiboranyl Platinum Triflate Complex as an Electrophilic Catalyst. *Organometallics* **2020**, *39*, 4169.

36. Wile, B. M.; Burford, R. J.; McDonald, R.; Ferguson, M. J.; Stradiotto, M. Neutral and Cationic Platinum(II) Complexes Supported by a P,N-Functionalized Indene Ligand: Structural and Reactivity Comparisons with a Related Gold(III) Zwitterion. *Organometallics* **2006**, *25*, 1028.

37. Fürstner, A.; Stelzer, F.; Szillat, H. Platinum-Catalyzed Cycloisomerization Reactions of Enynes. *J. Am. Chem. Soc.* **2001**, *123*, 11863.

38. Talley, M. R.; Stokes, R. W.; Walker, W. K.; Michaelis, D. J. Electrophilic activation of alkynes for enyne cycloisomerization reactions with in situ generated early/late heterobimetallic Pt–Ti catalysts. *Dalton Trans.* **2016**, *45*, 9770.

39. Hill, G. S.; Irwin, M. J.; Levy, C. J.; Rendina, L. M.; Puddephatt, R. J.; Andersen, R. A.; Mclean, L. Platinum (II) complexes of dimethyl sulfide. *Inorg. Synth.* **1998**, *32*, 149.

40. Bruker. **2019**, APEX3 (v2019.1.

41. Sheldrick, G. M. SADABS. University of Göttingen, Germany. **2016**.

42. Sheldrick, G. M. SHELXT - integrated space-group and crystal-structure determination. *Acta Crystallographica Section A* **2015**, *71*, 3.

43. Dolomanov, O. V.; Bourhis, L. J.; Gildea, R. J.; Howard, J. A. K.; Puschmann, H. OLEX2: a complete structure solution, refinement and analysis program. *J. Appl. Crystallogr.* **2009**, *42*, 339.

44. Frisch, M. J.; Trucks, G. W.; Schlegel, H. B.; Scuseria, G. E.; Robb, M. A.; Cheeseman, J. R.; Scalmani, G.; Barone, V.; Mennucci, B.; Petersson, G. A.et al.; *Gaussian 09*, Revision D.01, Gaussian, Inc., Wallingford, CT, 2013.

45. Glendening, E. D.; Landis, C. R.; Weinhold, F. NBO 6.0: Natural bond orbital analysis program. *J. Comput. Chem.* **2013**, *34*, 1429.